Journal of Hazardous Materials 178 (2010) 522–528

Contents lists available at ScienceDirect

Journal of Hazardous Materials

journal homepage: www.elsevier.com/locate/jhazmat

The thermal behaviour and structural stability of nesquehonite, $MgCO_3 \cdot 3H_2O$, evaluated by *in situ* laboratory parallel-beam X-ray powder diffraction: New constraints on CO_2 sequestration within minerals

Paolo Ballirano, Caterina De Vito, Vincenzo Ferrini, Silvano Mignardi *

Dipartimento di Scienze della Terra, Sapienza Università di Roma, P.le Aldo Moro 5, I-00185 Roma, Italy

ARTICLE INFO

Article history:
Received 18 November 2009
Received in revised form 20 January 2010
Accepted 21 January 2010
Available online 25 January 2010

Keywords:
Nesquehonite
Thermal behaviour
X-ray powder diffraction
Rietveld method
CO_2 sequestration

ABSTRACT

In order to gauge the appropriateness of CO_2 reaction with Mg chloride solutions as a process for storing carbon dioxide, the thermal behaviour and structural stability of its solid product, nesquehonite ($MgCO_3 \cdot 3H_2O$), were investigated *in situ* using *real-time* laboratory parallel-beam X-ray powder diffraction. The results suggest that the nesquehonite structure remains substantially unaffected up to 373 K, with the exception of a markedly anisotropic thermal expansion acting mainly along the *c* axis. In the 371–390 K range, the loss of one water molecule results in the nucleation of a phase of probable composition $MgCO_3 \cdot 2H_2O$, which is characterized by significant structural disorder. At higher temperatures (423–483 K), both magnesite and $MgO \cdot 2MgCO_3$ coexist. Finally, at 603 K, periclase nucleation starts and the disappearance of carbonate phases is completed at 683 K. Consequently, the structural stability of nesquehonite at high temperatures suggests that it will remain stable under the temperature conditions that prevail at the Earth's surface. These results will help (a) to set constraints on the temperature conditions under which nesquehonite may be safely stored and (b) to develop CO_2 sequestration *via* the synthesis of nesquehonite for industrial application.

1. Introduction

IPCC's Third Assessment Report [1] states that to stabilize the CO_2 concentration between 450 and 750 ppmv, cumulative emissions ranging from 220 to 2200 $GtCO_2$ (60–600 GtC) would need to be captured during this century. In this view, numerous approaches to CO_2 sequestration, including ocean, terrestrial, geological, biological and chemical options are currently being studied [2–10] and the retention or sequestration of CO_2 in geological reservoirs is currently the option being applied (e.g., Weyburn, Canada; Sleipner, North Sea [8]).

Technologies applied to CO_2 sequestration in mineral form, such as synthesis of minerals *via* reaction of CO_2 with Mg–Ca silicate rocks or of hydrated Mg carbonates in aqueous solutions, offer attractive options for the permanent and safe storage of CO_2 [11–15]. CO_2 sequestration by direct precipitation of carbonate minerals from solution, which represents a variant of the Solvay process [11], is based on carbonating alkaline brines to produce carbonate minerals from a chloride-rich solution. Carbon-capture technologies must (a) preserve the biological ecosystem, (b) warrant the stable trapping of CO_2, (c) be easily applicable also in developing countries and (d) ensure the formation of materials whose disposal in surface or underground does not involve environmental damage.

Recently, Ferrini et al. [16] described the reaction of gaseous CO_2 with $MgCl_2$ solutions that involved the precipitation of a low-temperature carbonate mineral, nesquehonite $MgCO_3 \cdot 3H_2O$. Various procedures for the synthesis of nesquehonite have been documented over the last century [17–20]. However, the novel method presented by Ferrini et al. [16] was aimed to be exploited as a CO_2 sequestering process and as a tool for disposing Mg-rich wastewater. Potential magnesium sources include seawater, artificial saltpans, and evaporitic saline deposits, but most of them are unsuitable for a cost-effective and energy-efficient process of CO_2 sequestration at present. In addition, these sources are only locally abundant to realistically be feed stock for the broad application of the carbonation process. However, they locally can represent feed stock for small-scale applications at industrial point sources. A massive supply of magnesium could be provided by saline aqueous wastes produced as a by-product of oil and gas production (the so-called "produced water" or "PW"), as well as reject brines from desalination process [21,22].

In order to model CO_2 mineral trapping within this mineral, it is essential to have a thorough understanding of the thermal behaviour of nesquehonite, the temperature range under which it is structurally stable, and the intermediate and final products of its

* Corresponding author. Tel.: +39 0649914836; fax: +39 064454729.
E-mail address: silvano.mignardi@uniroma1.it (S. Mignardi).

0304-3894/$ – see front matter © 2010 Elsevier B.V. All rights reserved.
doi:10.1016/j.jhazmat.2010.01.113

decomposition which may have lower CO_2:Mg ratios (i.e., due to partial loss of CO_2) [23,24].

Nesquehonite dissociation has been investigated mainly by thermal analysis [25–31]. Suzuki and Ito [32] monitored decomposition of nesquehonite coupling thermal analysis and X-ray diffraction and suggested that the structure of nesquehonite may be stable at least up to 343–353 K. The results by Ferrini et al. [16] extended the thermal stability of this carbonate up to 373 K.

A main feature of the differential thermal analysis (DTA) curve for nesquehonite is the presence of a sharp exothermic peak at about 500 °C, which has been attributed to the crystallization of magnesite ($MgCO_3$) or periclase (MgO) [28]. Ex situ X-ray powder diffraction patterns, collected after the quenching to room temperature (RT) of the samples (heated at temperatures corresponding to the discontinuities found in thermograms), lead to different intermediate and final products of nesquehonite decomposition. For a sample showing the strong exothermic peak, Hladky [28] reported the presence of amorphous material at 573 K and the occurrence of a phase of composition $MgO{\cdot}2MgCO_3$ at 743 K. Moreover, at 753 K, relatively well-crystallized magnesite was found, and at 873 K, well-crystallized periclase was found. On the contrary, in the case of a sample lacking the DTA exothermic peak, crystallization of periclase was observed to start at 743 K. Neither $MgO{\cdot}2MgCO_3$, nor magnesite was detected.

Therefore, there is a lack of detailed knowledge of the behaviour of nesquehonite structure at non-ambient conditions as this information can be acquired only by using *in situ* measurements.

In our first paper [16], we described the synthesis and the room temperature characterization of nesquehonite, whereas the present work represents the second part of this study and is devoted to investigate the thermal behaviour of nesquehonite and to characterize its decomposition process *in situ real-time* by non-ambient X-ray powder diffraction. These data provide new information that are of use in developing CO_2 storage within nesquehonite as an industrial process and may be used to facilitate modelling the storage of CO_2 within hydrated Mg-carbonate minerals.

2. Experimental methods

Nesquehonite was prepared following the procedure described in Ferrini et al. [16]. The experiments were carried out using both doubly distilled and tap water, high purity compressed CO_2 from SAPIO (Italy), and analytical grade reagents ($MgCl_2{\cdot}6H_2O$ and aqueous ammonia (25%) NH_3, Merck p.a.). Nesquehonite was synthesized by sparging CO_2 at about 100 mL/min through 200 mL of $MgCl_2{\cdot}6H_2O$ solution (about 7 g L^{-1} of Mg) at 20 ± 2 °C.

Ferrini et al. [16] provide more details concerning the experimental conditions and the full characterization of the synthetic nesquehonite by SEM, XRD, FTIR and thermal analyses.

For the *in situ* X-ray powder diffraction analysis, a 0.7 mm diameter SiO_2-glass capillary was filled with the nesquehonite powder and subsequently closed. The capillary was glued to a 1.2 mm diameter Al_2O_3 tube by means of a high-purity alumina ceramic (Resbond 989). The capillary/tube assembly was aligned onto a standard goniometer head and diffraction data were collected on a parallel-beam Bruker AXS D8 Advance, operating in transmission in θ–θ geometry. The instrument is fitted with an incident-beam Göbel mirror, a "position-sensitive detector" (PSD) VÅNTEC-1 set to a 6° 2θ aperture, and with a prototype of capillary heating chamber described by Ballirano and Melis [33–35].

The data were collected in step-scan mode over the 5–145° 2θ angular range (CuKα), using a step size 0.0219° 2θ and counting time of 1 s. A total of 101 isothermal measurements were carried out over the 303–803 K thermal range with a temperature step of 5 K. A magnified view of the complete data set is shown in Fig. 1.

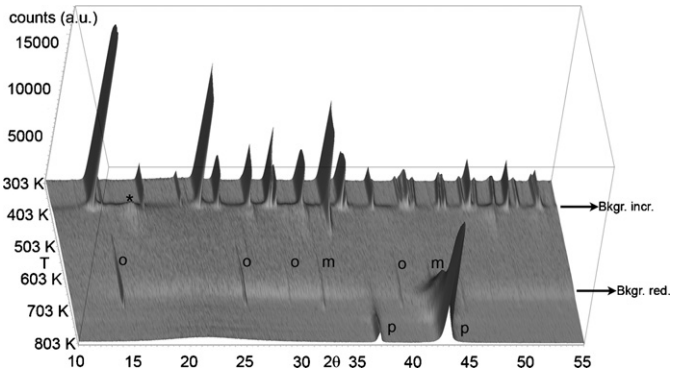

Fig. 1. Magnified view (10–55° 2θ) of the full data set of the heating cycle of nesquehonite shown as a 3D plot. Black arrows indicate background modification detectable as steps. The black star indicates the occurrence of an extra peak at 17° 2θ simultaneously to the smearing of all nesquehonite peaks except for 0 2 1 at 34° 2θ. Empty circles indicate peaks of the $MgO{\cdot}2MgCO_3$ phase. Peaks of magnesite are labeled with m and those of periclase with p.

Careful scrutiny of the RT pattern indicates the presence of traces of poorly crystallized hydromagnesite as can be seen from the presence of two clusters of reflections. These occur at about 15.2 (0 1 1, $\bar{1}$ 1 1) and 30.8° 2θ (0 2 2, 3 1 0) as broad, low intensity, peaks.

The data were evaluated by the Rietveld method by using the GSAS suite of programs [36] coupled with the EXPGUI graphical user interface [37]. Peaks shape was modelled by a Pseudo-Voigt function [38] modified to incorporate asymmetry [39]. Due to the presence of hydromagnesite peaks, regions $15 \leq {}^\circ 2\theta \leq 15.5$ and $30.6 \leq 2\theta \leq 31.3$ were excluded from structure refinements as no other intense peaks are overlapping with those of nesquehonite. Full Rietveld refinements were carried out for 55 diffraction patterns over the 303–373 and 608–803 K thermal ranges.

Preliminary scrutiny of the peak shape clearly indicated the occurrence of significant anisotropic peak broadening to be related to both the reported needle- or platelet-like morphology of nesquehonite [16,40] as well as to an anisotropic microstrain. However, a series of classic Williamson–Hall plots (scatter plots of $(\Gamma_{2\theta}/\cos\theta)$ vs $\sin\theta$) allowed identification of microstrain as the cause of the anisotropic broadening that was modelled using the Stephens approach [41]. Refined terms included S_{400}, S_{040}, S_{004}, S_{220}, S_{202}, S_{022}, and S_{103}.

The starting structure parameters were those reported by Giester et al. [40], space group $P2_1/n$, $Z = 4$, $a = 7.701$ Å, $b = 5.365$ Å, $c = 12.126$ Å, $\beta = 90.41°$. The structure refinements were carried out by imposing the following constraints derived from the reference RT structure investigations: C–O 1.285(10) Å, O–O 2.225(50) Å, Mg–O 2.075(40) Å, O–H 0.95(2) Å, H–H 1.515(30) Å, O···O 2.78(5) Å, except for the bifurcated O6···O1 and O6···O2, which were set to 3.075(100) Å. The statistical weight associated with those observations was reduced at each last refinement cycle leading to a final restraints contribution to the χ^2 never exceeding 2.4%. The isotropic displacement parameters were refined with those for O1 and O2 and O3, O4, and O5 constrained to be equal. The peak cut-off was set to 0.3% of the intensity of the strongest reflection of nesquehonite and background was fit with a 36-terms Chebyshev polynomial of the first kind. Following a well established procedure, such a large number of terms are required to properly model the broad bumps arising from the borosilicate-glass capillary. An absorption correction for cylindrical samples, including the contribution from the aluminium heating chamber windows, was determined at 303 K and kept fixed at that value for the non-ambient data. The evaluation of texture by means of a generalized spherical-harmonic description [42] was carried out according to a cylindrical sample symmetry using three parameters, 2 0 $\bar{2}$, 2 0 0, and 2 0 2. Refine-

Table 1
Miscellaneous data of refinements. Statistic indicators as defined in Young [53].

χ^2	1.293–1.433
R_{wp}%	5.27–5.52
R_p%	4.00–4.19
R_{Bragg}%	4.29–4.82
J	1.025–1.033
Refined parameters	104–105

ments confirmed the very limited presence of preferred orientation as a result of calculated texture indices J ranging from 1.025 to 1.033. As no modification of texture as a function of temperature was observed, an average value for each term was finally calculated and kept fixed at each temperature. The ranges of refinement statistics are listed in Table 1.

3. Results and discussion

3.1. Thermal decomposition of nesquehonite

The 3D plot (Fig. 1) clearly indicates the occurrence of a series of processes that will be described in detail in the following paragraphs and that may be summarized as follows:

(a) the diffraction pattern of nesquehonite remains relatively unaffected up to a T of 373 K. The pattern is virtually unchanged except for minor peak displacement arising from expansion of the unit cell;
(b) at 378 K, all peaks start to decrease in intensity except for 0 2 1, located at about 34° 2θ, which remains substantially unchanged;
(c) as temperature increases to 388 K, a broad extra peak (indicated by a black star in Fig. 1) starts to grow at about 17° 2θ. The occurrence of this peak is associated with a broadening of all peaks, except for the 0 2 1 peak of nesquehonite, and coupled with a marked increase in the intensity of the background;
(d) at 393 K, all peaks, except for 0 2 1, are replaced by broad bands. The background intensity reaches a maximum value. The intensity of all reflections start to decrease at 423 K until they disappear at 483 K;
(e) at 483 K, there is simultaneous growth of a new set of reflections that is followed by periclase nucleation at 603 K;
(f) at 653 K, periclase growth is associated with a marked reduction in the intensity of the background and a simultaneous reduction in the intensities of the remaining reflections;
(g) at temperatures higher than 683 K, only periclase reflections are present.

3.2. Rietveld refinements

Fractional coordinates and isotropic displacement parameters of non-hydrogen atoms at selected temperatures are reported in Table 2; the evolution of unit cell parameters and unit cell volume with increasing temperature is reported in Fig. 2; the thermal evolution of relevant bond distances and contacts is given in Fig. 3 and values for isotropic displacement parameters are given in Fig. 4.

Comparison of RT structural data with those reported in the literature [40] indicates an excellent agreement. However, unit cell parameters at elevated temperatures deviate from expected values. In fact, despite a regular increase of volume, they show a markedly anisotropic behaviour. The a cell parameter decreases slightly up to 323 K and subsequently shows a very limited increase, whereas the b cell parameter decreases regularly with increasing temperature. In both cases, the maximum variation is minimal, being of about 0.01 Å. Over the same temperature range, the c cell parameter shows a regular increase an order of magnitude greater with respect to the other cell parameters and the β angle decreases exponentially toward 90°. The maximum volume expansion, reached at the decomposition temperature is of ca. 0.6%. This anisotropic expansion is related to the structural features of nesquehonite, which consists of infinite ribbons running along the b axis. Each ribbon consists of MgO_6 octahedra linked to three CO_3 groups by two corners (O3 and O4) and one edge (O4′ and O5). Two water molecules, namely O1 and O2, complete the octahedral coordination. The adjacent ribbons are interconnected by hydrogen bonding. Such bonds are prevalently aligned along the c axis that, therefore, represents the "softest" direction of the structure.

Table 2
Fractional coordinates and isotropic displacement parameters (U_{iso}: Å^2) of non-hydrogen atoms of nesquehonite at selected temperatures. * constrained to be equal, ** constrained to be equal.

Site	T (K)	x	y	z	U_{iso}
Mg	308	0.2517(5)	0.0895(3)	0.14977(11)	0.0179(3)
	328	0.2526(6)	0.0914(3)	0.15003(11)	0.0184(3)
	348	0.2526(7)	0.0925(3)	0.15031(11)	0.0201(3)
	368	0.2537(6)	0.0948(3)	0.15047(11)	0.0207(3)
C	308	0.2505(11)	0.1393(5)	0.4079(2)	0.0264(14)
	328	0.2508(14)	0.1403(5)	0.4078(2)	0.0262(13)
	348	0.2503(15)	0.1404(5)	0.4077(2)	0.0282(14)
	368	0.2529(15)	0.1419(5)	0.4073(2)	0.0311(15)
O1	308	0.5208(3)	0.0900(5)	0.1518(2)	0.0331(5)*
	328	0.5221(3)	0.0884(5)	0.1509(2)	0.0356(5)*
	348	0.5212(3)	0.0865(5)	0.1504(2)	0.0374(5)*
	368	0.5219(3)	0.0874(6)	0.1501(3)	0.0396(5)*
O2	308	0.9816(3)	0.0964(6)	0.1476(2)	0.0331(5)*
	328	0.9824(3)	0.1020(6)	0.1494(2)	0.0356(5)*
	348	0.9817(3)	0.1087(6)	0.1505(3)	0.0374(5)*
	368	0.9823(3)	0.1126(6)	0.1508(3)	0.0396(5)*
O3	308	0.2653(6)	0.4093(4)	0.06276(16)	0.0168(3)**
	328	0.2705(6)	0.4109(4)	0.06300(16)	0.0164(3)**
	348	0.2710(7)	0.4113(4)	0.06324(16)	0.0177(3)**
	368	0.2729(6)	0.4141(4)	0.06367(16)	0.0188(3)**
O4	308	0.2484(7)	0.2053(4)	0.30587(16)	0.0168(3)**
	328	0.2516(9)	0.2079(4)	0.30589(15)	0.0164(3)**
	348	0.2514(9)	0.2090(4)	0.30585(15)	0.0177(3)**
	368	0.2464(9)	0.2114(4)	0.30589(16)	0.0188(3)**
O5	308	0.2526(6)	0.8164(3)	0.01962(16)	0.0168(3)**
	328	0.2550(8)	0.8176(3)	0.01988(15)	0.0164(3)**
	348	0.2584(8)	0.8185(3)	0.02080(15)	0.0177(3)**
	368	0.2576(9)	0.8209(3)	0.02129(16)	0.0188(3)**
O6	308	0.2735(5)	0.3517(4)	0.83842(17)	0.0356(9)
	328	0.2686(6)	0.3529(4)	0.83894(17)	0.0403(9)
	348	0.2675(6)	0.3524(4)	0.83969(17)	0.0428(9)
	368	0.2665(6)	0.3548(5)	0.84058(18)	0.0480(9)

The evaluation of the temperature dependence of bond distances (Fig. 4) indicates that Mg–O4 is the only one to show a regular increase. Analysis of the MgO_6 coordination polyhedra was carried out to calculate several geometrical parameters connected with the centroid of coordination [43]. Among those, only the volume distortion, defined as $\nu = (V_i - V_p)/V_i$ [44] where V_i and V_p are ideal and observed polyhedral volume, slightly increases with temperature from about 0.036 at 303 to 0.039 at 373 K. These parameters were calculated using the IVTON2 software (last version of the IVTON program of Balić-Žunic and Vickovic [43]). As expected, C–O bond distances are unaffected, at the 3σ level, within this limited thermal range.

The behaviour of the O···O contacts is more complex. Two of the seven O···O show a significant and regular increase in bond length. They are one of the two bifurcated O6–H5···O2 and O2–H3···O5 hydrogen bonds. On the contrary, the O1–H1···O5 hydrogen bond shortens. The remaining O···O contacts are substantially unchanged. Therefore, as expected, the mobility of the

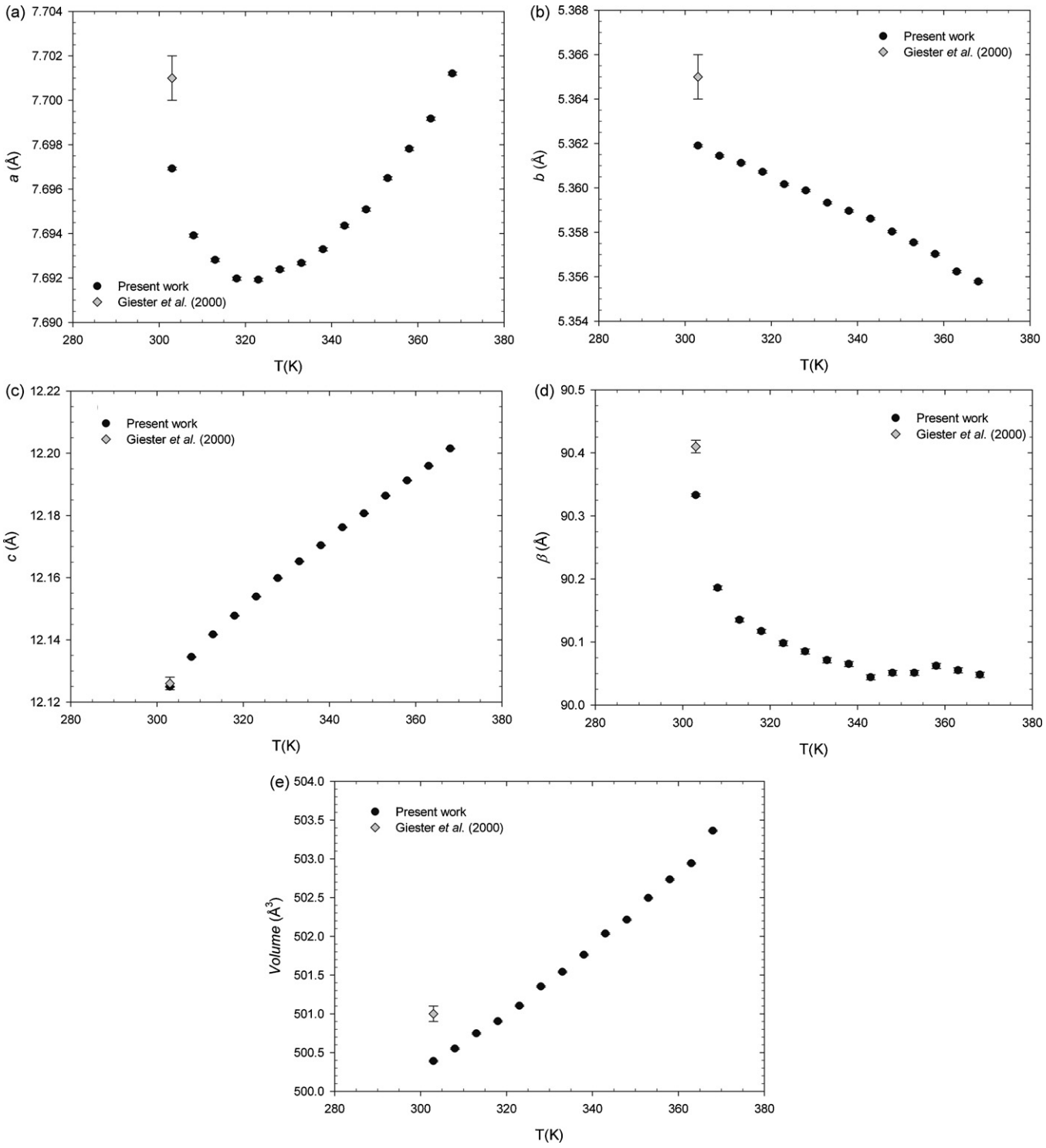

Fig. 2. Evolution of cell parameters and volume with temperature: (a) *a* cell parameter; (b) *b* cell parameter; (c) *c* cell parameter; (d) β angle; (e) volume; 95% confidence and prediction intervals are also reported.

"free water molecule" O6 plays a central role in the thermal behaviour of nesquehonite as confirmed by the more relevant increase of the corresponding U_{iso} isotropic displacement parameter as compared to the remaining atoms (Fig. 4).

Analysis of the temperature dependence of the strain-related peak broadening indicates only an increase of the S_{400} term, whereas the remaining terms show marginal variations.

At 378 K, all peaks of nesquehonite start to decrease in intensity except for 0 2 1, located at about 34° 2θ, that remains substantially unchanged. As temperature increases to 388 K a broad extra peak starts to grow at about 17° 2θ. This process is associated with a broadening of all peaks except for 0 2 1 and coupled with a marked increase in the intensity of the background. At 393 K, all peaks, except for 0 2 1, are replaced by broad bands, many of them at positions common to those of nesquehonite reflections. Fig. 5 compares the diffraction patterns collected at 373 and 418 K.

It is worth noting that Ferrini et al. [16] report endothermic steps at 371, 390, 417, and 493 K in their DTA measurements, according

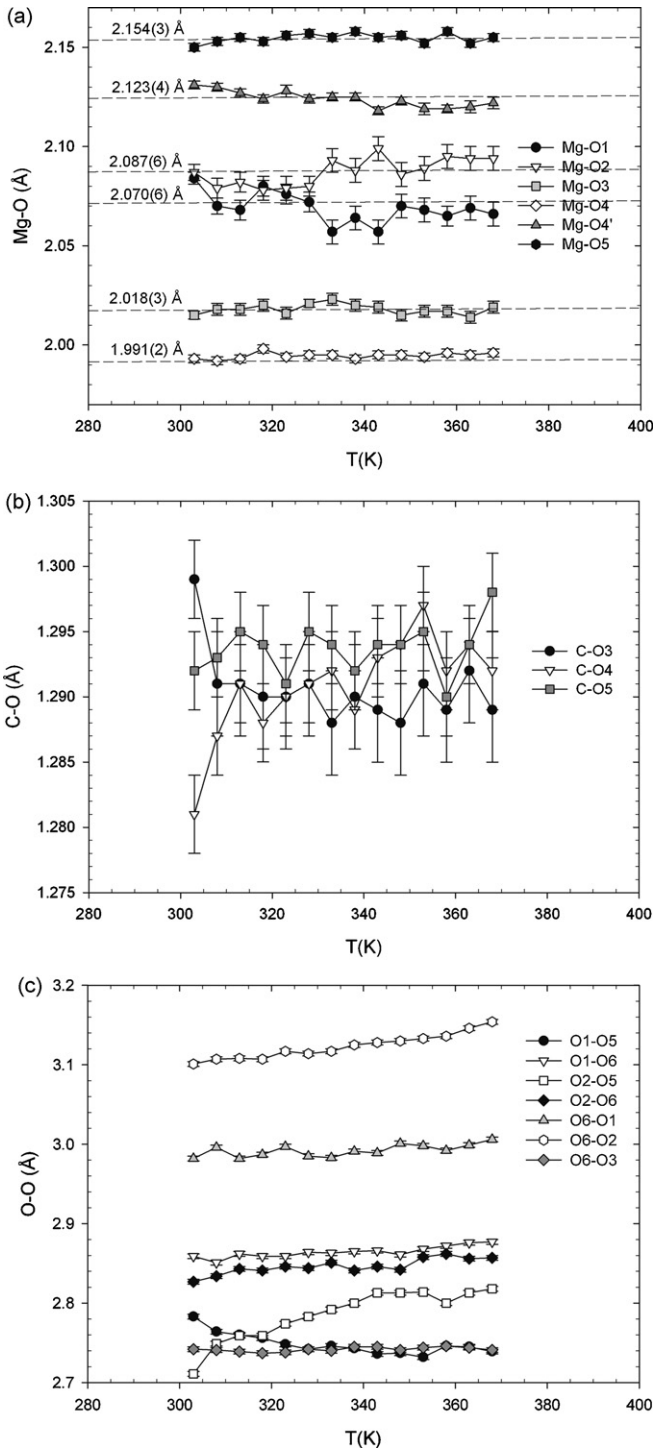

Fig. 3. Evolution of relevant bond distances and contacts with temperature: (a) Mg–O; (b) C–O; (c) O···O. Symmetry code: 1/2 − *x*, −1/2 + *y*, 1/2 − *z*.

to the results of previous studies [25–28,32]; slight discrepancies in the temperature of the endothermic steps can be ascribed to differences in experimental conditions. The first step is consistent with the start of the water loss process and the second to a total weight loss of about 14%, i.e., a single water molecule, based on the stoichiometry of nesquehonite. Coupling both X-ray and thermogravimetric data, it is possible to speculate that the modification of the diffraction pattern is related to the nucleation of a phase of possible composition $MgCO_3{\cdot}2H_2O$. Partial structural similarity seems to be assured by the presence of many common reflections, though

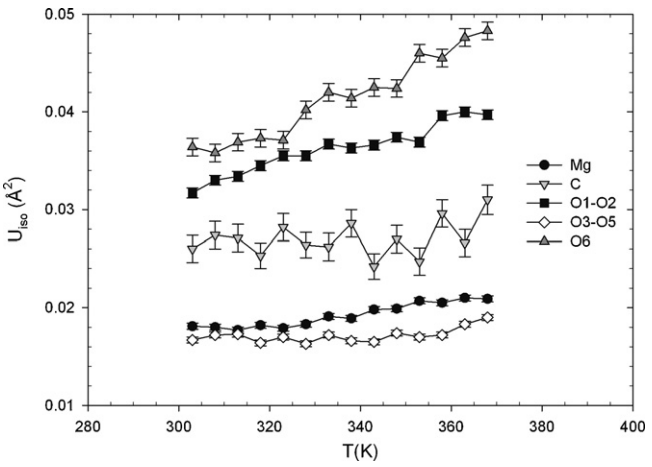

Fig. 4. Evolution of isotropic displacement parameters (U_{iso}: Å^2) with temperature. O1–5 refers to all oxygen atoms except for O6 ("free water molecule").

broadened. The presence of the narrow 0 2 1 reflection indicates that at least along such direction a regular structural coherency is preserved, whereas the broad bands and the increased background indicate the occurrence of a significant overall disorder. It is reasonable to speculate that the ribbon consisting of MgO_6 octahedra linked to three CO_3 groups, running along *b*, represents the preserved structural unit. However, it should be pointed out that there is no similarity with the *d*-spacings of barringtonite, $MgCO_3{\cdot}2H_2O$, reported by Nashar [45].

These peaks start to decrease in intensity at 423 K until complete disappearance at 483 K. They are simultaneously replaced by a new set of reflections involving those pertaining to magnesite (marked by an "m" in Fig. 1) and peaks located approximately at the same positions reported by Hladky [28] for $MgO{\cdot}2MgCO_3$ (identified in the same figure by an empty circle). However, this latter phase occurs at a temperature significantly lower than that reported in reference data [28]. This may be related to the different experimental set-up used as well as to differences in grain size. At 623 K, following Hladky [28] and hypothesizing a cubic structure, a cell parameter *a* of 8.56 Å was obtained from single-peak fitting. This cell parameter bears similarities with those of tetragonal phosgenite ($PbCl_2{\cdot}PbCO_3$) (a = 8.130(4) Å; c = 8.883(6) Å). Structural similarities could be hypothesized in the case of an $MgO{\cdot}MgCO_3$ composition instead of $MgO{\cdot}2MgCO_3$. Structural work on this nesquehonite decomposition product is currently in progress.

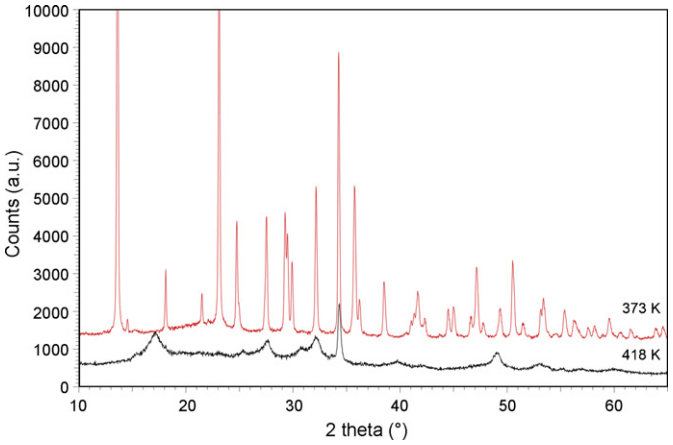

Fig. 5. Comparison of diffraction patterns collected at 373 and 418 K in the 10–65° 2θ range. A few common reflections persist albeit broadened whereas a few band appear at new 2θ positions.

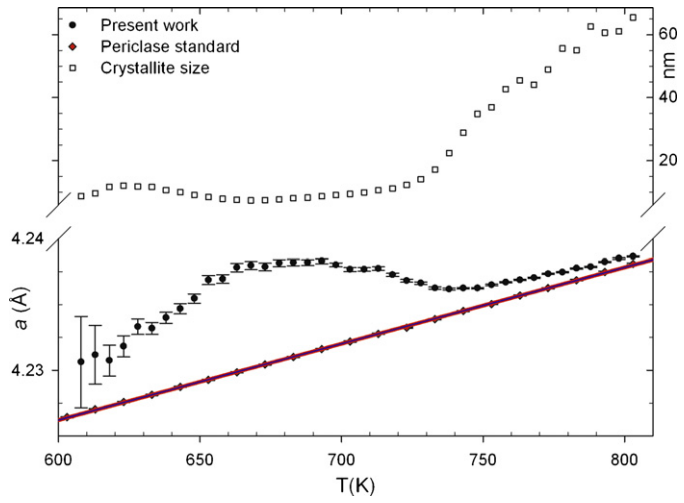

Fig. 6. Evolution of the periclase *a* cell parameter and crystallite size with temperature. For comparison purposes, the evolution within the same thermal range of the *a* cell parameter of a standard periclase sample has been reported.

At 603 K, periclase nucleation starts (peaks indicated by a "p" in Fig. 1). At 653 K, periclase becomes better crystallized (identified from peak sharpening) and the intensity of the background decreases abruptly (marked by an arrow in Fig. 1). The intensities of both magnesite and $MgO{\cdot}2MgCO_3$ reflections decrease until they disappear completely at 683 K.

Evaluation of the periclase *a* parameter (Fig. 6) and comparison with the evolution of the $1/\cos\theta$-dependent LX (Lorentzian crystallite size) profile parameter suggests a significant correlation. For comparison purposes, the *a* cell parameter of a periclase standard, used for thermocouple calibration, is also reported in Fig. 6. The *a* cell parameter of periclase obtained by the decomposition of nesquehonite is significantly larger than that of the standard and the differences increase as a function of LX. This implies that as the crystallite size of periclase decreases, approaching the nanoscale, the *a* cell parameter will increase beyond the value expected for well-crystallized periclase. This is in general agreement with the findings on nanosized iron oxides [46,47]. It is worth noting that the smallest refined crystallite size (~7 nm) (Fig. 6) is reached in correspondence of the digestion of both magnesite and $MgO{\cdot}2MgCO_3$.

3.3. Stability of nesquehonite in terms of temperature and solubility

The results of our study show that nesquehonite appears to be stable up to 373 K suggesting that its storage as "sequestering medium of CO_2" remains stable under the temperature conditions that prevail at the Earth's surface. Nevertheless, considering previous dated studies [27,32,48] which reported that nesquehonite may be structurally stable at least up to 70 or 80 °C, we consider safe its storage in suitable sites below this threshold. At temperature above 373 K the process of thermal decomposition of nesquehonite (*via* intermediate hydrated magnesium carbonate phases) ultimately produces magnesite in the range 423–483 K. This sequence involves the formation of carbonate minerals thermodynamically more stable than nesquehonite, resulting in a CO_2 storage stable for millions of years. Therefore, if the decomposition of nesquehonite would occur into underground storage facilities, this process further on would increase the safety of CO_2 disposal. The potential drawbacks of nesquehonite storage in underground could be represented by possible infiltration of water into the storage site as previous theoretical and experimental studies [27,48–52] showed that in solution the transformation of nesquehonite to hydromagnesite may occur at lower temperature than 373 K, depending on experiment duration. However, these experiments were performed imposing solid-to-solution mass ratio ranging from 4×10^{-2} to 9×10^{-2} [50], conditions which will not be reasonably reached when the location of the storage facility is carefully selected. Moreover, it is worth noting that some nesquehonite samples investigated in this study were synthesized by Ferrini et al. [16] and although stored at ambient conditions, they did not decompose within about three years. The same technical solutions in terms of thermal stability and solubility will be carefully considered when nesquehonite will be used for the production of building materials (e.g., aggregate in bricks, blocks, mortars and eco-cement concretes).

4. Conclusions

The thermal behaviour of nesquehonite and its dissociation process investigated *in situ* using *real-time* by non-ambient X-ray powder diffraction suggest the following conclusions:

(1) the appearance of the diffraction pattern of nesquehonite remains relatively unaffected up to 373 K;
(2) the thermal expansion of nesquehonite is markedly anisotropic because it occurs largely along the *c* axis of the crystal. This is due to the weak linkages between adjacent ribbons, built by MgO_6 octahedra and CO_3 groups, acting *via* hydrogen bonds prevalently aligned along this direction;
(3) in the range 371–390 K, one water molecule is lost and an unknown phase of possible composition $MgCO_3{\cdot}2H_2O$ nucleates;
(4) in the range 423–483 K, the peaks of the unknown phase decrease in intensity and are simultaneously replaced by a new set of reflections attributed to magnesite $MgCO_3$ and to a phase of possible composition $MgO{\cdot}2MgCO_3$;
(5) at 603 K, periclase nucleation starts and the reflections of both magnesite and $MgO{\cdot}2MgCO_3$ decrease in intensity until complete disappearance at 683 K.

These results clearly demonstrate that the nesquehonite storage requires no monitoring up to 373 K due to its thermal and structural stability as well as for the production of building materials. Finally, the evolution of the thermal treatment leads to the formation of magnesite, a carbonate thermally stable up to ~600 K, assuring the CO_2 stable storage for millions of years.

Acknowledgements

Financial support by Sapienza Università di Roma is acknowledged. Additional funding was provided by the Ministry of Education, University and Research (MIUR) through a National Research Program (PRIN 2006045331 001). The manuscript benefited considerably from the insightful and constructive reviews of JHM reviewers. All authors took part in the experimental work, the collection and analysis of the data, the interpretation of results and the preparation of this paper.

References

[1] T. Morita, J. Robinson, A. Adegbulugbe, J. Alcamo, D. Herbert, E.L. Rovere, N. Nakicenovic, H. Pitcher, P. Raskin, K. Riahi, A. Sankovski, V. Sololov, H.J.M. Vries, Z. Dadi, Greenhouse gas emission mitigation scenarios and implications, in: B. Metz, O. Davidson, R. Swart, J. Pan (Eds.), Climate Change 2001: Mitigation, Contribution of Working Group III to the Third Assessment Report of the Intergovernmental Panel on Climate Change, Cambridge University Press, Cambridge, 2001, pp. 115–166.
[2] N. Assayag, J. Matter, M. Ader, D. Goldberg, P. Agrinier, Water–rock interactions during a CO_2 injection field-test: implications on host rock dissolution and alteration effects, Chem. Geol. 265 (2009) 227–235.

[3] M. Fernández Bertos, S.J.R. Simons, C.D. Hills, P.J. Carey, A review of accelerated carbonation technology in the treatment of cement-based materials and sequestration of CO_2, J. Hazard. Mater. 112 (2004) 193–205.
[4] P. Freund, W.G. Ormerod, Progress toward storage of carbon dioxide, Energy Convers. Manage. 38 (1997) 199–204.
[5] D. Georgiou, P.D. Petrolekas, S. Hatzixanthis, A. Aivasidis, Absorption of carbon dioxide by raw and treated dye-bath effluents, J. Hazard. Mater. 144 (2007) 369–376.
[6] B. Metz, O. Davidson, H. de Coninck, M. Loos, L. Meyer (Eds.), Carbon Dioxide Capture and Storage, IPCC Special Report, Cambridge University Press, Cambridge, 2005, pp. 1–433.
[7] S. Holloway, An overview of the underground disposal of carbon dioxide, Energy Convers. Manage. 38 (1997) 193–198.
[8] S. Holloway, J.M. Pearce, V.L. Hards, T. Ohsumi, J. Gale, Natural emissions of CO_2 from the geosphere and their bearing on the geological storage of carbon dioxide, Energy 32 (2007) 1194–1201.
[9] E. Rendek, G. Ducom, P. Germain, Carbon dioxide sequestration in municipal solid waste incinerator (MSWI) bottom ash, J. Hazard. Mater. 128 (2006) 73–79.
[10] I.M. Power, S.A. Wilson, J.M. Thom, G.M. Dipple, J.E. Gabites, G. Southam, The hydromagnesite playas of Atlin, British Columbia, Canada: a biogeochemical model for CO_2 sequestration, Chem. Geol. 206 (2009) 302–316.
[11] K.S. Lackner, Carbonate chemistry for sequestering fossil carbon, Annu. Rev. Energy Environ. 27 (2002) 193–232.
[12] W.K. O'Connor, D.C. Dahlin, G.E. Rush, C.L. Dahlin, W.K. Collins, Carbon dioxide sequestration by direct mineral carbonation: process mineralogy of feed and products, Miner. Metall. Proc. 19 (2002) 95–101.
[13] D. Daval, I. Martinez, J. Corvisier, N. Findling, B. Goffé, F. Guyot, Carbonation of Ca-bearing silicates, the case of wollastonite: experimental investigations and kinetic modelling, Chem. Geol. 265 (2009) 63–78.
[14] F. Dufaud, I. Martinez, S. Shilobreeva, Experimental study of Mg-rich silicates carbonation at 400 and 500 °C and 1 kbar, Chem. Geol. 265 (2009) 79–87.
[15] M.C. Hales, R.L. Frost, W.N. Martens, Thermo-Raman spectroscopy of synthetic nesquehonite—implication for the geosequestration of greenhouse gases, J. Raman Spectrosc. 39 (2008) 1141–1149.
[16] V. Ferrini, C. De Vito, S. Mignardi, Synthesis of nesquehonite by reaction of gaseous CO_2 with Mg chloride solution: its potential role in the sequestration of carbon dioxide, J. Hazard. Mater. 168 (2009) 832–837.
[17] F.A. Genth, S.L. Penfield, On Lansfordite, Nesquehonite, a new mineral, and pseudomorphs of Nesquehonite after Lansfordite, Am. J. Sci. 39 (1890) 121–137.
[18] M. Hänchen, V. Prigiobbe, R. Baciocchi, M. Mazzotti, Precipitation in the Mg-carbonate system-effects of temperature and CO_2 pressure, Chem. Eng. Sci. 63 (2008) 1012–1028.
[19] J.T. Kloprogge, W.N. Martens, L. Nothdurft, L.V. Duong, G.E. Webb, Low temperature synthesis and characterisation of nesquehonite, J. Mater. Sci. Lett. 22 (2003) 825–829.
[20] K.M. Towe, P.G. Malone, Precipitation of metastable carbonate phases from seawater, Nature 226 (1970) 348–349.
[21] L.E. Kanagy, B.M. Johnson, J.W. Castle, J.H. Rodgers Jr., Design and performance of a pilot-scale constructed wetland treatment system for natural gas storage produced water, Bioresour. Technol. 99 (2008) 1877–1885.
[22] J.A. Veil, M.G. Puder, Regulatory Considerations in the Management of Produced Water—A US perspective, Produced Water Management-Gas TIPS, 2005, pp. 25–28.
[23] J.H. Canterford, G. Tsambourakis, B. Lambert, Some observations on the properties of dypingite, $Mg_5(CO_3)_4(OH)_2{\cdot}5H_2O$, and related minerals, Miner. Mag. 48 (1984) 437–442.
[24] S.A. Wilson, M. Raudsepp, G.M. Dipple, Verifying and quantifying carbon fixation in minerals from serpentine-rich mine tailings using the Rietveld method with X-ray powder diffraction data, Am. Miner. 91 (2006) 1331–1341.
[25] N. Morandi, La dissociazione termica dell'idromagnesite e della nesquehonite, Miner. Petrogr. Acta 15 (1969) 93–108.
[26] R.C. Mackenzie, Differential Thermal Analysis, Academic Press, London, 1970.
[27] P.J. Davies, B. Bubela, The transformation of nesquehonite into hydromagnesite, Chem. Geol. 12 (1973) 289–300.
[28] G. Hladky, $MgO{\cdot}2MgCO_3$, an intermediate product of the thermal decomposition of nesquehonite, Neues Jb. Miner. Monatsh. 3 (1975) 115–120.
[29] M. Dong, Z. Li, J. Mi, G.P. Demopoulos, Solubility and stability of nesquehonite ($MgCO_3{\cdot}3H_2O$) in mixed $NaCl + MgCl_2$, $NH_4Cl + MgCl_2$, LiCl, and $LiCl + MgCl_2$ solutions, J. Chem. Eng. Data 54 (2009) 3002–3007.
[30] R.L. Frost, M.C. Hales, W.N. Martens, Thermogravimetric analysis of selected group (II) carbonate minerals—implication for the geosequestration of greenhouse gases, J. Therm. Anal. Calorim. 94 (2008) 1–7.
[31] V. Vágvölgyi, M. Hales, R.L. Frost, A. Locke, J. Kristóf, E. Horváth, Conventional and controlled rate thermal analysis of nesquehonite $Mg(HCO_3)(OH){\cdot}2(H_2O)$, J. Therm. Anal. Calorim. 94 (2008) 523–528.
[32] J. Suzuki, M. Ito, Nesquehonite from Yoshikawa, Aichi Prefecture, Japan: occurrence and thermal behaviour, J. Jpn. Assoc. Miner. Petrol. Econ. Geol. 69 (1974) 275–284.
[33] P. Ballirano, E. Melis, Thermal behaviour of β-anhydrite $CaSO_4$ to 1,263 K, Phys. Chem. Miner. 34 (2007) 699–704.
[34] P. Ballirano, E. Melis, Thermal behaviour and kinetics of dehydration of gypsum in air from in-situ-real-time laboratory parallel-beam X-ray powder diffraction, Phys. Chem. Miner. 36 (2009) 391–402.
[35] P. Ballirano, E. Melis, The thermal behaviour of γ-$CaSO_4$, Phys. Chem. Miner. 36 (2009) 319–327.
[36] A.C. Larson, R.B. Von Dreele, GSAS—General Structure Analysis System, Los Alamos National Laboratory Report No. LAUR 86-748, Los Alamos National Laboratory, Los Alamos, 2000.
[37] B.H. Toby, EXPGUI, a graphical user interface for GSAS, J. Appl. Crystallogr. 34 (2001) 210–213.
[38] P. Thompson, D.E. Cox, J.B. Hastings, Rietveld refinement of Debye–Scherrer synchroton X-ray data from Al_2O_3, J. Appl. Crystallogr. 20 (1987) 79–83.
[39] L.W. Finger, D.E. Cox, A.P. Jephcoat, A correction for powder diffraction peak asymmetry due to axial divergence, J. Appl. Crystallogr. 27 (1999) 892–900.
[40] G. Giester, C.L. Lengauer, B. Rieck, The crystal structure of nesquehonite, $Mg(CO_3){\cdot}3H_2O$, from Lavrion, Greece, Miner. Petrol. 70 (2000) 153–163.
[41] P.W. Stephens, Phenomenological model of anisotropic peak broadening in powder diffraction, J. Appl. Crystallogr. 32 (1999) 281–289.
[42] R.B. Von Dreele, Quantitative texture analysis by Rietveld refinement, J. Appl. Crystallogr. 30 (1997) 517–525.
[43] T. Balić-Žunic, I. Vickovic, IVTON—program for the calculation of geometrical aspects of crystal structures and some crystal chemical applications, J. Appl. Crystallogr. 29 (1996) 305–306.
[44] T. Balić-Žunic, Use of three-dimensional parameters in the analysis of crystal structures under compression, in: A. Grzechnik (Ed.), Pressure-induced Phase Transitions, Transworld Research Network, Kerala, India, 2007, pp. 157–184.
[45] B. Nashar, Barringtonite—a new hydrous magnesium carbonate from Barrington Tops, New South Wales, Australia, Miner. Mag. 34 (1965) 370–372.
[46] M. Di Marco, M. Port, P. Couvreur, C. Dubernet, P. Ballirano, C. Sadun, Structural characterization of Ultrasmall Superparamagnetic Iron Oxide (USPIO) particles in aqueous suspension by Energy Dispersive X-ray Diffraction (EDXD), J. Am. Chem. Soc. 128 (2006) 10054–10059.
[47] M. Di Marco, P. Ballirano, M. Port, E. Piscopiello, P. Couvreur, C. Dubernet, C. Sadun, Atomic pair distribution function (PDF) study of iron oxide nanoparticles in aqueous suspension, J. Mater. Chem. 19 (2009) 6354–6360.
[48] D. Langmuir, Stability of carbonates in the system $MgO–CO_2–H_2O$, J. Geol. 73 (1965) 730–754.
[49] E. Königsberger, L.C. Königsberger, H. Gamsjäger, Low-temperature thermodynamic model for the system $Na_2CO_3–MgCO_3–CaCO_3–H_2O$, Geochim. Cosmochim. Acta 63 (1999) 3105–3119.
[50] Y. Xiong, A.S. Lord, Experimental investigations of the reaction path in the $MgO–CO_2–H_2O$ system in solutions with various ionic strengths, and their applications to nuclear waste isolation, Appl. Geochem. 23 (2008) 1634–1659.
[51] A. Botha, C.A. Strydom, Preparation of a magnesium hydroxy carbonate from magnesium hydroxide, Hydrometallurgy 62 (2001) 175–183.
[52] L. Hopkinson, K. Rutt, G. Cressey, The transformation of nesquehonite to hydromagnesite in the system $CaO–MgO–H_2O–CO_2$: an experimental spectroscopic study, J. Geol. 116 (2008) 387–400.
[53] R.A. Young, Introduction to the Rietveld method, in: R.A. Young (Ed.), The Rietveld Method, Oxford Press, 1993, pp. 1–38.